

Modelling the Manufacturing History, Through Life Creep-Fatigue Damage and Limiting Defect Sizes of a Pipework Joint using Finite Element Based Methods

M J Stevens¹, Dr R J Dennis², I J M Bottomley³ and Dr R A W Bradford⁴

¹ Frazer-Nash Consultancy Limited, 1 Trinity Street, College Green, Bristol, BS1 5TE, UK, m.stevens@fnc.co.uk, Tel: +44 (0)117 922 6242, Fax: +44 (0)117 922 6524

² Frazer-Nash Consultancy Limited, 1 Trinity Street, College Green, Bristol, BS1 5TE, UK, r.dennis@fnc.co.uk

³ Frazer-Nash Consultancy Limited, Stonebridge House, Dorking, RH4 1HJ, UK, i.bottomley@fnc.co.uk

⁴ EDF Energy Nuclear Generation Limited, Barnett Way, Bamwood, Gloucester, GL4 3RS, UK, rick.bradford@edfenergy.com

Abstract

The work reported in this paper describes a simulation of the manufacture, through-life operation and limiting defect size assessment of a pipework joint in a nuclear powerplant boiler. The objective of this work is to understand the critical factors that influence the integrity of the joint in-service and support accurate predictions of service life. This work differs from typical structural integrity assessments in that advanced modeling techniques have been used through-out the assessment process and include detailed simulations of the manufacturing process, a simulation of the entire in-service operating history including predictions of creep-fatigue damage and cracked body analysis to determine limiting defect sizes.

Residual stresses resulting from the manufacturing process can be a key driver for creep and creep-fatigue damage. The calculation of creep-fatigue damage for assessment purposes is typically undertaken within the framework of an appropriate assessment code, such as EDF Energy's R5. The standard assessment approach usually requires calculation of stresses using elastic finite element analysis followed by hand calculations to calculate the damage.

A combination of explicit and implicit finite element methods are employed to simulate a range of manufacturing processes which influence the in-service structural integrity of a branched pipework joint. Where available, test data have been compared to the results to assess the validity of the simulation. The simulation results then feed into a finite element based structural integrity assessment. The methods follow the principles outlined in the EDF Energy R5 assessment code but use the inelastic strains calculated directly from analysis. The methods are based around the general purpose finite-element code Abaqus.

The residual stresses generated during manufacture may adversely affect the critical defect sizes for the pipework joint. However, the complex geometry and loading complicate the assessment of the cracked body. Therefore, a finite-element analysis representing the cracked body has been carried out on the pipework joint to evaluate the J-Integrals at the locations of interest and hence calculate the critical defect sizes. The analysis considers the residual stresses determined from the finite-element analysis of the manufacturing processes.

Keywords: Creep-fatigue damage, finite element analysis, residual stress, J-Integral, cracked body mesh

1. Introduction

The objective of this work is to understand the critical factors that influence the structural integrity of a pipework joint in-service and support accurate predictions of service life. This work differs from typical structural integrity assessments in that advanced modeling techniques have been used through-out the assessment process and include detailed simulations of the manufacturing process, a simulation of the entire in-service operating history including predictions of creep-fatigue damage and cracked body analysis to determine limiting defect sizes.

Residual stresses resulting from the fabrication process can be a key influencing factor for creep and creep-fatigue damage. Welded components can develop significant residual stresses before they enter service, but are typically ignored when predicting the service lives of components. Additionally cold forming processes that are undertaken prior to welding introduce additional residual stresses and furthermore Post-Weld Heat Treatment (PWHT) may significantly reduce these stresses whilst at the same time introducing creep damage. The influence of the manufacturing process on in-service integrity is therefore a complex phenomena.

Residual stresses that are generated by manufacturing processes cannot be accurately determined using simple calculations. Therefore, Finite Element (FE) simulations were performed in order to predict the magnitude of plastic strains material state and therefore residual stress. The processes modeled included pipe bending, pipe flaring/swaging and cutting of weld excavations along a complex weld path with a varying cross-section. A two pass moving heat source welding simulation was performed for the component weld, with the geometry of the component determined directly by the cold forming processes and the material in the cold formed state, in order to predict the welding residual stresses. An FE simulation of the subsequent PWHT was performed in order to predict the relaxation of stresses and accumulated creep damage throughout the component. Where available, test data have been compared to the results to assess the validity of the simulation.

In-service creep-fatigue damage was predicted by further FE analysis. As well as the consideration of service loads, the remnant residual stresses and hardened material state from the manufacturing history were included as an input to the stress state within the component. The methods applied the principles outlined in the EDF Energy R5 assessment code, which is described in more detail in Section 2, but used the inelastic strains calculated directly from FE analyses.

The same residual stresses may adversely affect the maximum defect size that the component can withstand whilst subjected to in-service loads. However, the complex geometry and loading complicate the assessment of the cracked body. Therefore, FE analysis was carried out on the pipework joint to evaluate the J-Integrals at the locations of interest and hence calculate the critical defect sizes.

2. Calculation of Creep-Fatigue Damage Based Upon R5 Principles

The calculation of creep-fatigue damage for assessment purposes is typically undertaken within the framework of the R5 assessment code (Reference 1). The standard assessment approach is to undertake elastic FE followed by Neuber construction to convert elastic stress ranges into elastic-plastic stress and strain ranges prior to the calculation of creep-fatigue damage.

The intention of this work was to perform non-linear finite element analyses accounting for elastic-plastic and creep deformation to determine the magnitudes of the inelastic strains directly. The methods followed the principles outlined in R5 (Reference 1) but used the in-elastic strains calculated directly from FEA. The methods were based around the use of the user-defined subroutines CREEP and UVARM.

The creep damage increment at any point is defined as the time integral of the ratio of the accumulated equivalent creep strain to the material creep ductility, so that crack initiation would be predicted when the ductility is exhausted and the damage level reaches unity.

The creep damage per cycle, d_c , is defined as:

$$d_c = \int_0^{t_h} \frac{\dot{\bar{\epsilon}}_c}{\bar{\epsilon}_f(\dot{\bar{\epsilon}}_c)} dt \quad (1)$$

where t_h is the duration of the creep dwell, $\dot{\bar{\epsilon}}_c$ is the instantaneous creep strain rate during the dwell and $\bar{\epsilon}_f(\dot{\bar{\epsilon}}_c)$ is the appropriate creep ductility, taking account of the effects of stress state and creep strain rate.

The following key points should be noted with regard to the calculation of fatigue damage:

- The calculation of the total strain range is based upon the components of elastic, $\Delta\bar{\epsilon}_{el}$, plastic, $\Delta\bar{\epsilon}_{pl}$, and creep strain, $\Delta\bar{\epsilon}_{cr}$, which are summated to give the total range, $\Delta\bar{\epsilon}_t$. A volumetric strain enhancement is not applied since this is implicitly accounted for within the finite element approach;
- A Fatigue Strength Reduction Factor (FSRF) was not included on the basis that its effects were predominantly accounted for within the finite element approach. The dominant effect of the FSRF is in regard to a Weld Strain Enhancement Factor (WSEF) and resulting enhancement to fatigue damage, which is indeed covered within the finite element approach. However a FSRF can be considered to be the combined effect of a WSEF and also a Weldment Endurance Reduction (WER). The WER should still be applied in this instance since it relates to fatigue damage. The WER was not applied in this simulation. However, fatigue damage in this work is generally negligible and so the absence of a WER, which is a relatively modest correction, was considered acceptable;
- The fatigue endurance data is adjusted for size effects based upon the thickness of the thinnest section, which in this case is the wall of the 1.5" pipe (4mm).

3. Description of Component

The component is a pipework joint which combines the flow of superheated steam from two inlet tubes into a single outlet tube. The pipework joint is made by bending a length of tube through an angle of 150° and cutting off the extrados of the bend to leave an oval opening (Figure 1). A transition stub made from type 316H stainless steel is swaged at one end to match this opening and the two parts are joined by welding. The bent tubing is 1.5" (38.1mm) outside diameter and 8G (4.06mm) wall thickness and the swaged tube is 2" (50.8mm) outside diameter and 5G (5.38mm) wall thickness.

PWHT was applied. The weld caps were not dressed.

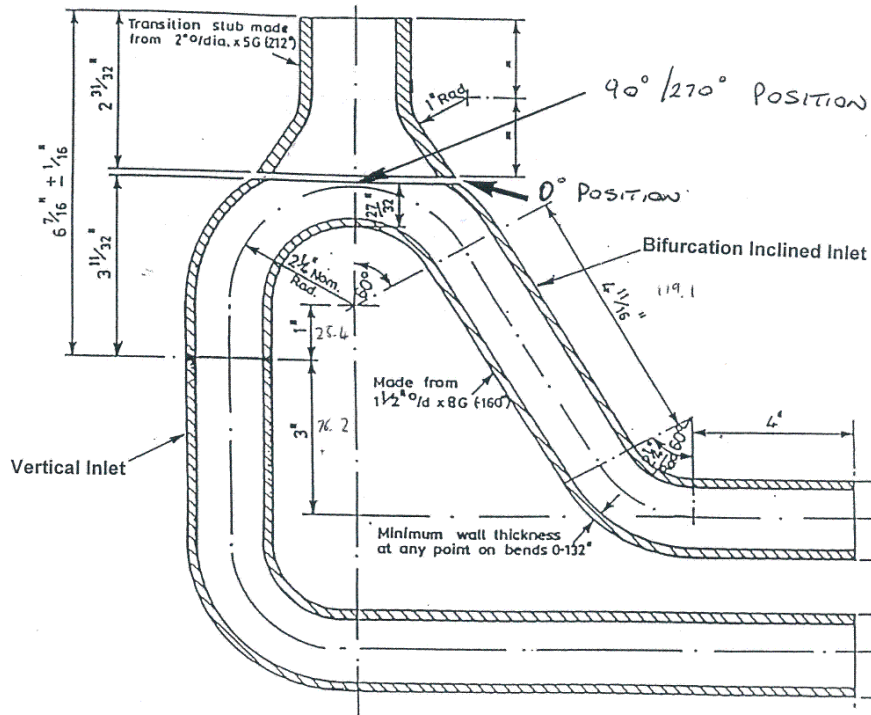


Fig. 1. Pipework Joint

4. Simulation Methodology

The simulation was performed in the following steps using Abaqus FE analysis software (Reference 2):

1. **Cold forming:** This step was used to calculate the plastic strains and residual stresses generated within the component by the processes used to cold form the pipe prior to welding. Three processes were involved: cold bending of the 1.5" pipe, swaging of the 2" pipe and machining the weld excavation;
2. **Welding:** This step was used to calculate the residual stresses generated during welding and subsequent treatment. Prior to this step being carried out, the stress and strain solutions to Step 1 were imported into the model. At the end of this step, the residual stress field represented the stress state at the start of operational life. Three processes were simulated in this step: welding, PWHT and pressure proof testing;
3. **In-Service Operation:** This step was used to calculate the creep-fatigue initiation damage by simulating in-service behaviour throughout the lifetime of the component. The solutions from the preceding steps were imported into the model to represent the residual stress field and material state at the start of operational life;
4. **Cracked Body Analysis:** A cracked-body FE analysis was performed to evaluate the J-Integrals for a range of postulated defect sizes. The J-Integrals were used to determine the critical defect sizes in the joint for the loading observed in-service. The analysis considered the residual stress field generated during the manufacturing process (Steps 1 and 2).

Finite element simulations were performed using Abaqus/Explicit (Reference 2) to simulate the cold bending of the 1.5" pipe and cold swaging of the 2" pipe. The solutions were then imported into Abaqus/Standard for subsequent simulation of the springback, machining, welding, heat treatment, in-service operation and cracked body analysis.

5. Material Properties

This section describes the material properties used for the FE models.

5.1. Physical Properties

The pipework joint was manufactured using Type 316H Stainless Steel tube material and 316L Stainless Steel weld metal. Young's modulus and Poisson's ratio for 316H parent and 316L weld material were taken from Reference 3.

The behavior of the material under thermal loading is described by the specific heat capacity, conductivity and thermal expansion. These properties were assumed to be identical for parent and weld metal and were taken from Reference 4.

5.2. Hardening Model

The analyses presented here used a constitutive material hardening law based upon the Lemaitre-Chaboche formulation provided within Abaqus. The Lemaitre-Chaboche formulation is described here; however the following points should be noted:

- Reference 5 provides generic recommendations for the application of material hardening laws in welding simulations. The hardening parameters for both parent and weld metal were supplied by EDF Energy. For information the hardening model is referred to as the "mixed-ff" Type 316 model in Reference 5;
- The hardening parameters were based upon monotonic and isothermal cyclic tensile test programmes on Type 316H parent metal and Type 316L weld metal;
- The parent hardening model followed the generic recommendations (Reference 5) apart from the fitting of the isotropic parameter, Q_{∞} , which was adjusted according to the magnitude of the specific 1.0% proof strength of the material at 20°C (364.5MPa best estimate);
- The weld hardening model was based upon a model derived for Type 316L SS weld metal (Reference 5);
- Plastic strain annealing was accounted for using a two stage annealing process.

The Lemaitre-Chaboche hardening model implemented within Abaqus was divided into kinematic and isotropic hardening components. The kinematic portion was defined using the relationship:

$$\dot{\alpha} = C \frac{1}{\sigma^0} (\sigma - \alpha) \dot{\epsilon}^{pl} - \gamma \alpha \dot{\epsilon}^{pl} \quad (2)$$

Where $\dot{\alpha}$ is the rate of change in kinematic back stress, σ^0 is the size of the yield surface (MPa), $\dot{\epsilon}^{pl}$ is the equivalent plastic strain rate and C, γ are fitting coefficients (MPa and dimensionless respectively).

C is the initial kinematic hardening modulus, and γ determines the rate at which the hardening modulus decreases with increasing plastic deformation. C varies with temperature, but γ was defined as constant over the entire temperature range.

The isotropic portion (i.e. the size of the yield surface) was defined via a simple exponential law:

$$\sigma^0 = \sigma|_0 + Q_\infty \left(1 - e^{-b\bar{\epsilon}^{pl}}\right) \quad (3)$$

Where Q_∞ and b are material parameters, $\bar{\epsilon}^{pl}$ is the equivalent plastic strain and $\sigma|_0$ is the size of the yield surface at zero plastic strain (MPa).

Note that the assignment of parent and weld material properties was determined based on the maximum temperature that an element would reach during the entire analysis. All elements which exceed a temperature of 1400°C were assigned weld metal properties due to weld pool mixing. The remaining elements were assigned parent metal properties.

5.3. Creep Properties

Creep deformation was modelled by the RCC-MR empirical law for primary and secondary creep of AISI Type 316 austenitic stainless steel. In order to incorporate tertiary creep, the creep damage level was incorporated into the creep deformation law in such a way as to increase the strain rate asymptotically to infinity as the creep damage level reached unity. This was achieved by factoring the creep rate by the ratio $1/(1-d^3)$, where d is the creep damage. In practice the result was a doubling in the creep rate once a damage of 0.8 has been achieved with the creep rate tending to infinity when d tended towards unity.

The PWHT was carried out at a temperature of 1050°C. Guidance on RCC-MR creep deformation parameters is only provided as far as 700°C within the British-Energy R66 Code (Reference 6). Therefore it was necessary to extrapolate the creep deformation parameters up to 1050°C, making use of the available test data up to 900°C.

The uniaxial ductility of the Type 316 SS parent material and HAZ was assumed to be strain rate and temperature dependent as described in Reference 7. The properties exhibit an increase in lower shelf ductility at temperatures above 550°C. A constant uniaxial creep ductility of 3.5% was assumed for the weld material (Reference 8), which is independent of both temperature and strain rate.

6. Finite Element Models

This section describes the finite element models that have been developed to carry out the simulations described above. In total five models were used to predict respectively the bent 1.5" pipe plastic pre-strain, swaged 2" pipe plastic pre-strain, welding residual stresses, creep-fatigue damage accumulation and cracked body analysis. The models were constructed using Abaqus/CAE (Reference 2).

6.1. Cold Forming Models

The finite element meshes of the cold forming models were constructed from eight node three-dimensional brick elements. Linear reduced integration elements were used (Abaqus type C3D8R). Forming dies were represented with rigid shell elements (Abaqus type R3D4). The models representing the 1.5" bent pipe and 2" swaged pipe are shown in Figure 2 and 3.

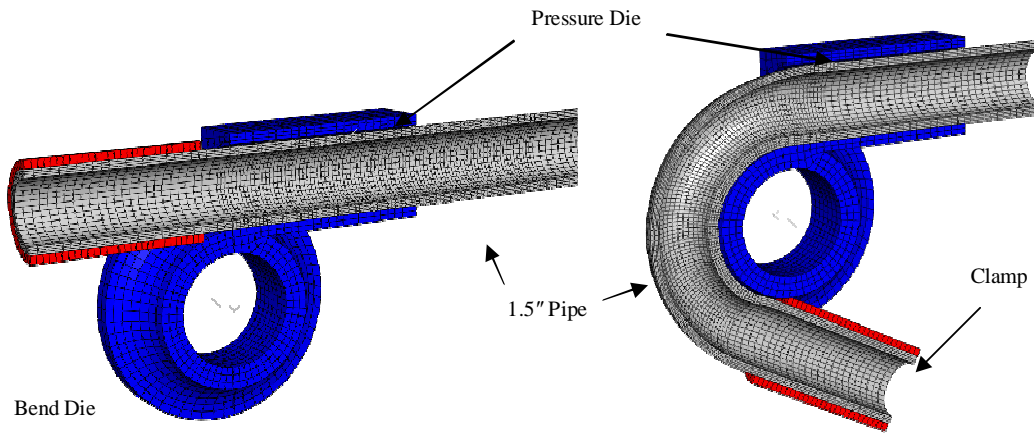


Fig. 2. 1.5" Pipe Cold Forming (Bending) Finite Element Model

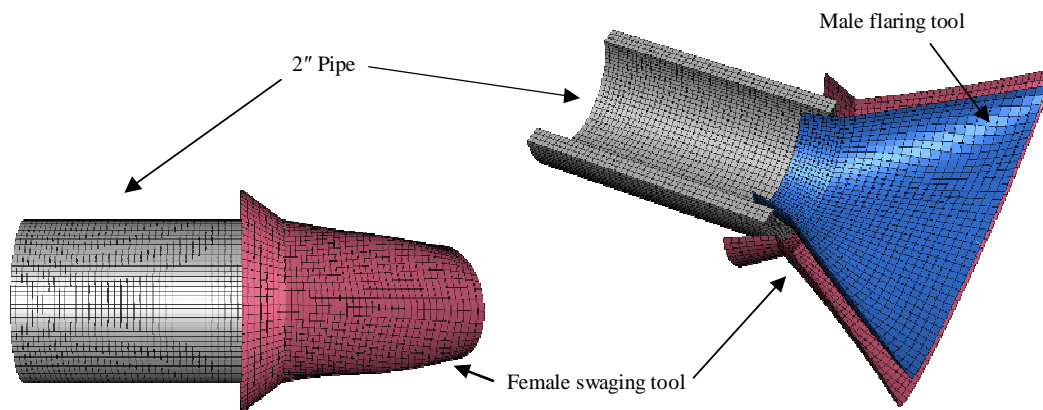


Fig. 3. 2" Pipe Cold Forming (Swaging) Finite Element Model

A structured mesh was generated for both pipe models. The 1.5" bent pipe model is more refined within the bend region, with larger elements towards the ends of the pipe. The simulation modelled the action of the Hilger bending machine, which uses a bend die, a pressure die, a clamp and a boost die in order to force the pipe into a bend.

The 2" pipe swaging simulation modelled a male and female ram forming process. Simultaneously a male tool flares the pipe in one direction, whilst a female tool swages the pipe in the other. The shapes of the tools were chosen such that they forced the cross-section of the 2" pipe to match the shape of the cut in the extrados of the bent 1.5" pipe.

6.1.1. Cold Bending of the 1.5" Pipe

The plastic strain generated in the 1.5" pipe following the bending process needs to be accounted for prior to welding. A finite element simulation was performed using Abaqus/Explicit (Reference 2) to simulate the bending of the 1.5" pipe.

The 1.5" pipe was bent through 150° and cut at its extrados near the apex of the bend, providing the dual inlets to the pipework joint. The bending was performed as shown in Figure 2.

Contact between the 1.5" pipe and forming dies in Abaqus was modelled as surface-to-surface contact interactions using the penalty contact method with finite sliding. For the clamp, a rough friction formulation was employed that allowed no tangential slip. Other surfaces were modelled as above with a friction coefficient of 0.06 representative of lubricated steel on steel (Reference 9).

6.1.2. Cold Swaging of the 2" Pipe

In a similar manner to the 1.5" pipe it was necessary to predict the plastic strain generated in the 2" pipe as a result of the swaging process. The purpose of the swaging was to flare the pipe so that its cross-section matched the shape of the cut in the extrados of the bent 1.5" pipe. This provides the outlet from the pipework joint. Simultaneously a male tool flared the pipe in one direction, whilst a female tool swaged the pipe in the other (Figure 3).

Note that the plastic strains due to both cold forming processes (i.e. swaging and bending) harden the parent material prior to welding, and hence influence the residual stresses developed during welding. Both cold forming models were exported from Abaqus/Explicit into Abaqus/Standard in order to perform a static springback analysis. The forming dies were removed and the pipes were effectively unrestrained as an equilibrium step was performed.

6.1.3. Cutting of the Extrados and Weld Excavation

The bent 1.5" pipe and 2" pipe were brought together to form the pipework joint. This involved cutting a section from the extrados of the bent 1.5" pipe in order to allow an outlet to the 2" pipe (Figure 4). The pipes were welded together at their interface, which involved the cutting of a weld excavation profile on both the 1.5" and 2" pipes. The angle of the excavation side wall varied around the weld path on either side as shown in Figure 4.

The cuts of both the extrados and the weld excavation were simulated by mapping the results of the cold forming analyses to a new FE model. In order to facilitate this mapping process, the geometry of the new model was identical to that of the deformed shape from the swaging and bending models. The key features of the new model are that the 2" pipe and 1.5" pipe are brought together, and material is removed from the regions that are cut.

The material state (plastic pre-strain, hardening and residual stress) from the cold forming was mapped onto the new model. The mapping procedure used three Abaqus/Standard (Reference 2) user subroutines (HARDINI, SIGINI and SDVINI). Results were not mapped into the regions where material was removed, since this effectively modeled, in a single step, the removal of material due to machining of the weld excavation. The result was subject to an equilibrium step in order to capture any stress redistribution as a result of material removal. It was assumed that the free ends of the pipework joint were restrained in preparation for welding when the cut was made.

6.2. Welding Model

The finite element mesh of the pipework joint was constructed from twenty node three-dimensional brick elements. Reduced integration hybrid elements (Abaqus type C3D20RH) were used. The hybrid formulation prevented the elements becoming over constrained (element 'locking') in regions of high plastic strain.

The mesh was biased towards the weld both across the surface and through the thickness. It was designed to become coarser moving away from the weld as much as possible with minimal discontinuities in the size or aspect ratio of adjacent elements, and with no warped elements. The service simulation mesh was refined

from the welding mesh, since creep-fatigue damage prediction requires a finer mesh to avoid significant discontinuities.

The weld consists of a root pass and a filler pass (Figure 4). Both passes consist of two beads each, where each bead starts and stops at the crotch locations and spans 180° around the weld excavation.

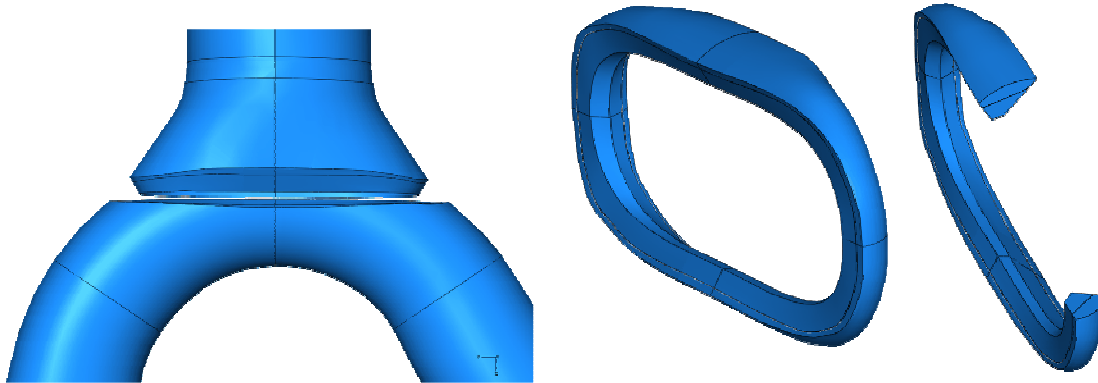


Fig. 4. Element Parent and Weld Geometry

For the welding model (Figure 5 and 6), the root pass had 4 elements through the bead height whilst the filler pass had 2 elements through the bead height (i.e. 6 elements through-thickness in total). There were 4 elements across the weld and 176 elements around the length of the weld.

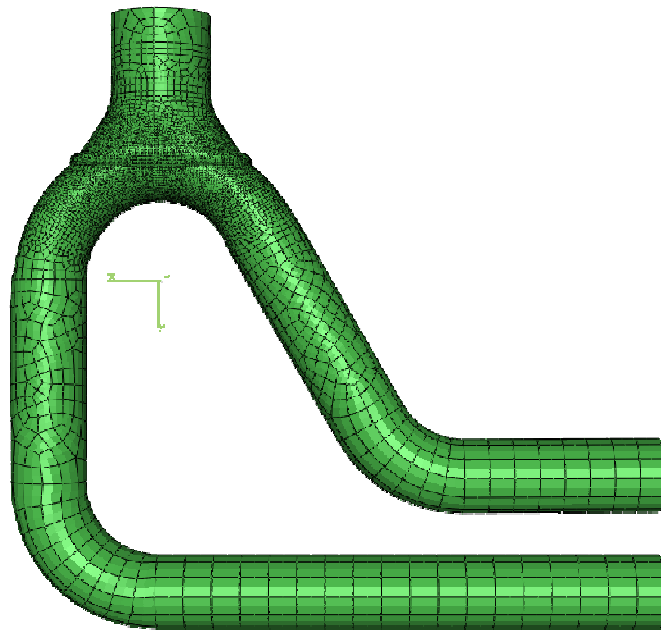


Fig. 5. Welding Mesh

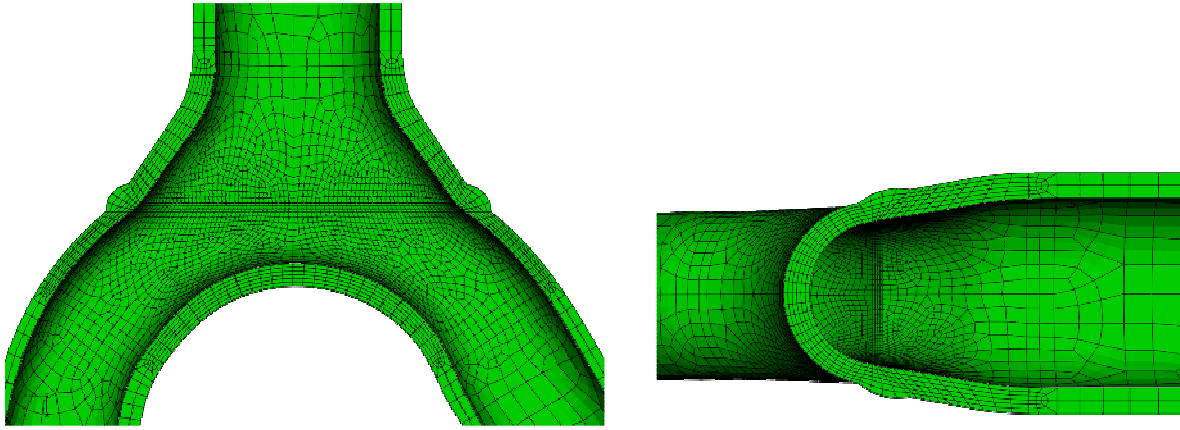


Fig. 6. Welding Mesh Detail

For the service simulation model (Figure 7), the root pass had 5 elements through the bead height whilst the filler pass had 3 elements through the bead height. There were 6 elements across the weld and 200 elements around the length of the weld.

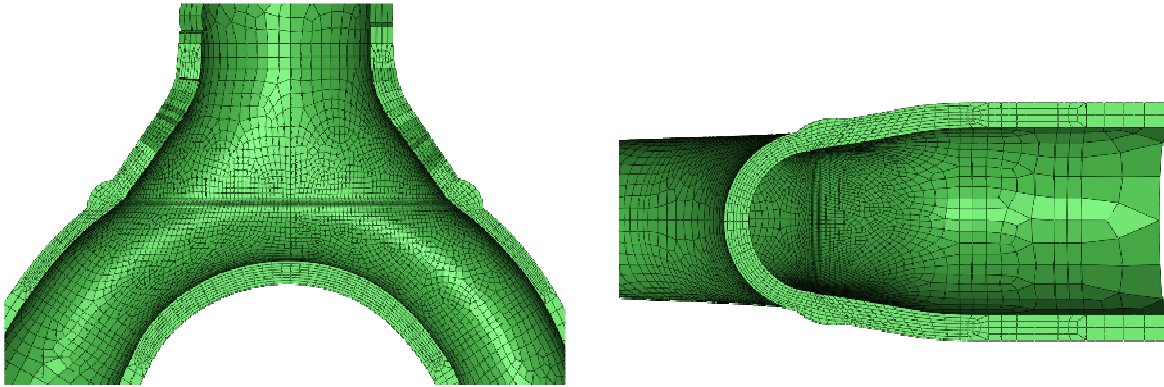


Fig. 7. Service Simulation Mesh Detail

6.2.1. Plastic Strain Annealing

The temperature transient loadings associated with simulating the welding process introduce large non-linear strains into the welded structure. These strains are typically treated as plastic strains in present simulation methods. However, in real stainless steel materials, creep deformation begins to become important above 450°C and dominates behavior above around 850°C. In addition, above 800°C historically accumulated plastic strains start to be annealed as recovery and re-crystallisation temperatures are approached. When temperatures reach the material melting point the plastic strains are annealed entirely.

The default annealing functionality incorporated into Abaqus is both simple and relatively crude. This was replaced by a two stage functionality implemented in a user subroutine using the UHARD facility within Abaqus (Reference 2). Using this method, the material ceases to harden isotropically above a lower annealing

temperature T1, but does not lose any prior isotropic hardening unless the upper annealing temperature, T2, is exceeded. The lower annealing temperature was set at 950°C and the upper annealing temperature at 1300°C for both parent and weld.

6.2.2. Welding

The 1.5" pipe and 2" pipe were welded together at their interface in order to create the pipework joint. The weld consisted of one root pass followed by a capping pass, both laid down using a manual Tungsten Inert Gas (TIG) process. Each of the passes consisted of two 180° weld beads with start and stop positions located at the crotches. The weld was not dressed.

A sequentially coupled thermal-mechanical analysis using Abaqus/Standard (Reference 2) was performed to simulate the welding. An appropriate thermal analysis method was selected. In reality stress raisers are observed at weld bead start and stop locations which are not modelled when using a traditional simultaneous bead deposition welding technique. For the analysis presented in this paper each of the weld passes was modelled using a moving heat source technique with each pass made up of two 180° weld beads. The initial thermal modelling was carried out using the Heat Source Modelling Tool (HSMT) (References 10 & 11), which was used to calibrate a thermal solution at cross-sections along the weld path. The full moving heat source analysis was carried out using Abaqus/Standard. The model (Section 6.2) was allowed to cool to an inter-pass temperature of 150°C between each bead. It was then allowed to cool to ambient temperature on completion of the last pass.

6.2.3. Heat Inputs

The cross-sectional area, normal to the advance direction, of weld metal deposited by Manual TIG welding was assumed directly proportional to the electrical heat input per unit length.

The weld pass areas were calculated by measuring the total area of weld metal deposited from macrographs of ex-service and mock-up components. On average these were found to be 40mm². The total weld area was divided between the root and filler passes in proportion with their assumed electrical heat inputs.

The welding process, filler wire diameters and input currents were obtained from the welding specification. The filler wire diameters and input currents were chosen to be the minimum values of their respective ranges from the weld specification for the root pass, and the maximum values in the range for the filler pass. This was consistent with a representative increase in weld area from the root to the filler pass.

The weld excavation varies in its chamfer angle around the excavation cut (Figure 4), from 0° to 30° for the 1.5" pipe side, and from 45° to 60° on the 2" pipe side. This caused the excavation to open and close up around the weld. As it did so, the weld cap varied in height in order to maintain the constant 40mm² cross-sectional area.

6.2.4. Moving Heat Source

The size of the volumetric heat source modelled within both the HSMT and Abaqus was assumed to be the same size as the electrode used. The path of the moving heat source followed the geometric centre of the instantaneous weld pass cross-section in the torch travel direction. Due to the high aspect ratio of the bead, weaving was represented in the filler pass. Weaving was accounted for by stretching the shape of the heat source into an ellipsoid of increased lateral diameter. This diameter was consistently 125% of the bead width (at mid-height) along the weld path. The variation with time of bead width, torch position, torch travel direction and lateral stretch angle was accounted for in the analysis. Welding efficiencies of 65% and 60% were used for the root and filler pass respectively.

The volumetric heat source was defined within the Abaqus user-defined DFLUX subroutine. This subroutine was provided so that Abaqus users can define complex heat fluxes, in this case dependent on spatial position and time. The heat input for the moving heat source was represented by an ellipsoidal distribution defined by the non-dimensional effective torch radius, r_e (that is the distance from the torch centre, which is non-dimensionalised with respect to the heat source dimensions):

$$r_e = \sqrt{\left(\frac{x}{r_x}\right)^2 + \left(\frac{y}{r_y}\right)^2 + \left(\frac{z}{r_z}\right)^2} \quad (4)$$

where (x, y, z) is a dynamic Cartesian co-ordinate system centred on the weld torch that translates and rotates with the torch. x follows the torch advance direction, y is the instantaneous through-thickness direction and z is the instantaneous transverse direction. r_x , r_y and r_z are the instantaneous radii of the elliptical heat source in the x , y and z directions respectively, which can vary with time in the transverse direction to simulate weaving.

The volumetric heat input, q , was assigned to reduce from the torch position by a Gaussian function based on the effective torch radius:

$$q = K_q e^{-r_e^2} \quad (5)$$

where K_q was defined so that the total heat flux deposited upon integration in the finite element model equalled the effective power from the torch.

Thermal isolation ahead of the torch was achieved in Abaqus using material properties with a field variable dependence. Ahead of the torch the weld bead was defined as inactive with a field variable of 2. For all material points with a field variable of 2 the conductivity was reduced by 2 orders of magnitude to ensure adequate isolation of the inactive weld bead. For all weld material points with a field variable of 1, the material properties were not adjusted and depended solely on temperature. Where the field variable was between 2 and 1 (i.e. just ahead of the torch in the Gaussian scaling region) the properties were linearly interpolated to ensure a smooth variation. Note that when the two root beads were being deposited, the two filler beads were isolated by being entirely removed from the model, using the *MODEL CHANGE option in Abaqus (Reference 2). Following the deposition of the second root bead and on reaching the interpass temperature, the filler beads were added into the model solution.

Field variables were calculated within the Abaqus user-defined UFIELD subroutine and updated at each nodal position. This subroutine was provided so that Abaqus users can define complex field variable distributions, in this case dependent on the torch position and updated as the torch moved through the model.

6.2.5. Mechanical Response

The mechanical analysis was a continuation of the cutting simulation, using the same finite element model. Elements were activated sequentially in order to represent each weld bead. Thermal expansion was driven by the transient temperature distribution calculated in the thermal analysis. The mechanical analysis was carried out using Abaqus/Standard.

The inlet ends, remote from the weld and influence of any high temperatures, were fully fixed to model the mechanical restraint in place at these ends. During fabrication the inlet ends were temporarily welded to each other with a small plate.

6.2.6. Post Weld Heat Treatment

The welded component was joined to the plant pipework, at which stage the assembly underwent a solution heat treatment. Measurement of ex-service component delta ferrite levels were consistent with a PWHT conforming to the fabrication specification as follows:

1. Heat at 250°C /hour to 1050°C;
2. Hold at 1050°C for 15 minutes;
3. Cool at 3000°C /hour to ambient.

The PWHT was carried out in nitrogen and a rapid cool-down was achieved by quenching in cold nitrogen gas. Free air cooling was applied once 300°C was reached.

A finite element simulation was carried out using Abaqus/Standard to predict the relaxation of welding stresses and accumulation of creep damage during PWHT. The finite element mesh was refined (and the material state was mapped) from the weld simulation. This was due to damage predictions requiring a finer mesh to avoid significant result discontinuities.

The transient temperatures were applied isothermally to the model using the heating and cooling rates defined above. The free air-cooling below 300°C was neglected since it is below the creep regime.

Creep damage was calculated during PWHT and subsequent in-service simulation using a dedicated Abaqus user subroutine applicable for 316 stainless steels.

6.2.7. Pressure Proof Testing

When the component was connected to the plant pipework, it was subjected to an in-shop 3,924 psig hydraulic pressure proof test following heat treatment.

A further pressure test was performed before the component enters service. With closure welds made, the boiler as a whole was subjected to a 3,300psig pressure test on-site.

These pressure tests were simulated as step changes in pressure applied to the inside surface of the pipework joint model. These finite element analysis steps were a continuation of the PWHT simulation.

6.3. In-Service Operation Model

This section describes the FE model used to analyse the in-service behaviour of the pipework joint and hence determine the creep-fatigue damage accumulated throughout the operational lifetime.

6.3.1. Operating Conditions

A representative service history was required to simulate the in-service operating conditions experienced by the pipework joint from commissioning, to date, and in the future to 45 years operation.

Two cycle types were considered in the analysis: Cold Shutdown (CSD) and Hot Standby (HSB) cycles.

The classification of a CSD and a HSB cycle is presented in Table 1:

Table 1. Classification of CSD and HSB cycles

Cold shutdown cycle	Hot standby cycle
100% normal operation	100% normal operation
Dwell period	Dwell period
Quadrant or Reactor trip / Overpressure	Quadrant or Reactor trip / Overpressure
Interim hot shutdown	Hot shutdown
Cold shutdown	

A total of 35 CSD and 350 HSB cycles over the 30 years of operation were modelled. This represented a dwell period of approximately 545 hrs.

6.3.2. System Loadings

Normal operation system loadings due to boiler expansion and rotation were applied as forces and moments at the two component inlet ends. During operation the system loadings relax as the boiler pipework creeps. This relaxation was accounted for by scaling the forces and moments applied to the pipework joint over time in proportion with the relaxation of the dominant moment acting on the pipework from Reference 12.

During a cold shutdown, the system loadings were reduced by a constant amount equal to the initial elastic load range. Therefore, the system loads were of reversed sign when shutdown, due to creep relaxation during normal operation. The stress range between normal operation and the HSB condition was 62% of the stress range between normal operation and the cold shutdown condition.

The pipework joint was fully restrained at the outlet end, providing reaction forces that balance the system loads applied at the two inlet ends.

6.3.3. In-Service Creep-Fatigue Damage

The pipework component was subjected to a variety of load cycles through the first thirty years of operation. A finite element simulation was carried out using Abaqus/Standard to predict the through life accumulation of creep damage during operating periods and fatigue damage during hot standby and cold shutdown cycles over the first 30 years of operation.

The FE analysis was a continuation of the pressure proof test analyses, containing the material state (plastic pre-strain, hardening and residual stress) resulting from the manufacturing history.

Service loadings due to the boiler expansion and rotation were applied to the pipework joint model. The calculation of creep-fatigue damage defined in the R5 (Reference 1) procedure was integrated into the damage prediction subroutines of the FE analysis.

6.4. Cracked Body Model

The intention of the cracked body analyses was to model a defect that had formed in-service after the steady cyclic stress state had been established. Therefore, an elastic-plastic analysis was performed and the effect of the residual stresses in the J-Integral evaluation therefore needed to be considered.

The 90° (flank) position was chosen for calculating the limiting defect sizes since the maximum stresses during operation were calculated at that location. Five different crack sizes were modelled. The crack aspect ratio was not constant and was estimated by fitting a curve to actual crack size data from components removed from service and sectioned.

It was assumed that cracks propagated through the wall in a direction perpendicular to the bifurcation wall and therefore through the thinnest section. As this direction varies around the weld perimeter, the crack faces were not planar.

The uncracked mesh described in Section 5 was modified to develop separate cracked meshes for each crack size. The cracked meshes were generated using Zencrack Version 7.4, which simplified the complex process of developing a three-dimensional focused mesh by replacing identified elements with crack blocks. Each crack block contained a refined focused mesh with a section of crack front. The cracked mesh for a 2.3 mm deep defect at the flank location is shown in Figure 8.

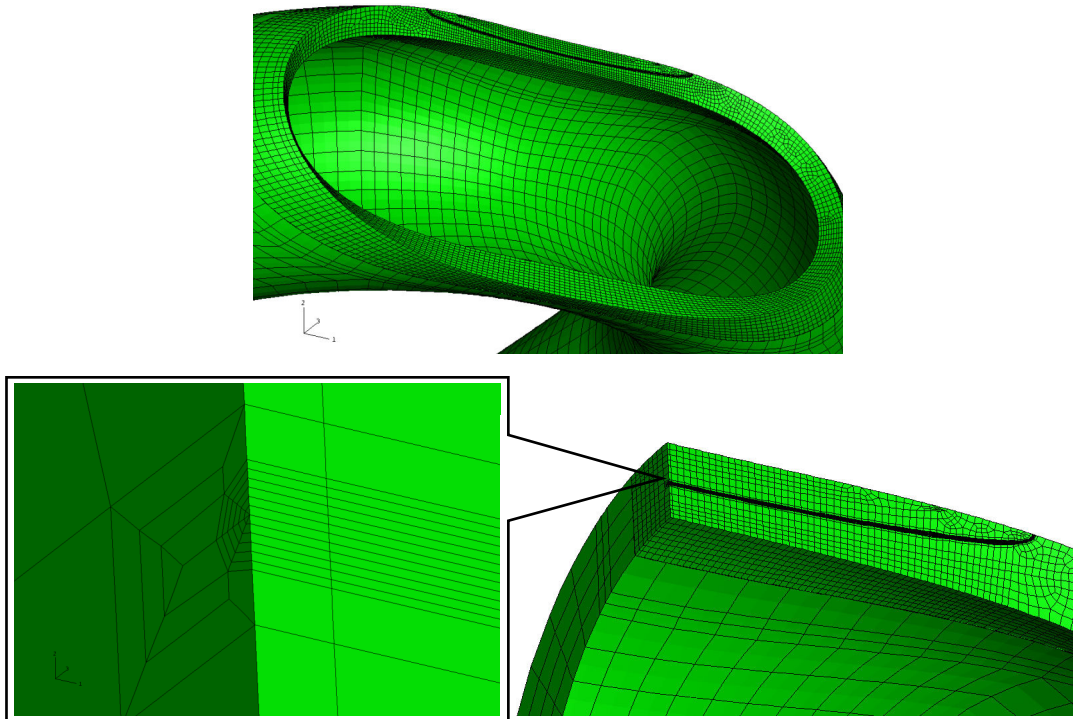


Fig. 8. Detail of the cracked mesh for the flank defect, modelled using Zencrack software

For each node along the crack front, Zencrack creates outputs for seven virtual crack extension (VCE) directions. These directions are spaced at 20° intervals from 60° below the crack face to 60° above the crack face, as shown in Figure 9.

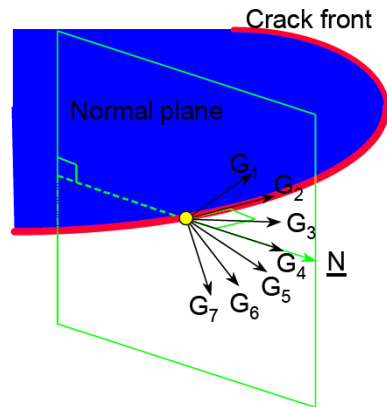


Fig. 9. Virtual crack extension directions

Whilst the crack was assumed to grow perpendicular to the bifurcation wall (direction G_4 in Figure 9), this was not necessarily the most onerous case and crack stability was assumed to be controlled by the direction of the maximum J-Integral. The J-Integral was therefore evaluated for all seven VCE directions.

The analysis was elastic-plastic. Therefore, the crack tip was modelled as a r^{-1} singularity by permitting the crack tip nodes formed by the collapsed elements to move independently to 'blunt' the crack tip. The mid-side nodes remained at their mid-side locations.

6.4.1. Assessing the Effect of Residual Stresses on the J-Integrals

The residual stresses calculated using the FE models described in Section 5 were mapped from the uncracked mesh onto the cracked mesh. The mapping was carried out from an undeformed mesh onto an undeformed mesh.

The residual stress and material hardening information was transferred using the *MAP SOLUTION keyword in Abaqus (Reference 2). After the stresses were mapped across, an additional step without loading was required to allow the model to find equilibrium due to small numerical errors in transferring the stress and strain data. During the mapping and equilibrium steps, the crack was kept closed.

The evaluation of J-Integrals within Abaqus is only valid for monotonic loading and will not calculate correct contour integrals for analyses that include initial stresses (Reference 2). Therefore, EDF Energy provided the post processing software JEDI for evaluating the J-Integrals from the stresses and strains derived from the Abaqus cracked FE models.

The suitability of JEDI as a post processing tool was determined by comparing the evaluation of J-Integrals with Abaqus for a model that did not contain a residual stress field. The comparison is not reported in detail here. In summary, for simple elastic analyses, similar results were calculated between JEDI and Abaqus. However, the JEDI J-Integral evaluations are sensitive to the mesh density, mesh quality and selected large or small displacements (NLGEOM 'on' or 'off' respectively) and are generally less robust than the Abaqus evaluation method. However, it was concluded that JEDI was suitable for considering the relative sensitivity of the results to the residual stresses.

To ensure an appropriate comparison, the same cracked mesh was used with and without residual stresses. The following approach was used to evaluate the JEDI results including residual stress. Note that Steps 1 and 2 were not carried out for calculating the J-Integrals without residual stress:

- Step 1 – Map residual stresses from the model described in Section 5 to the cracked mesh with the crack face tied shut;
- Step 2 – Equilibrium step without load, crack closed;
- Step 3 – Apply 100% normal operating system loads + full external pressure load (3.9 MPa, including crack face pressure) + 50% normal operating steam pressure (prevents overclosure of the crack), crack closed;
- Step 4 – As step 3 but with the crack open;
- Step 5 – Perform a series of analyses with increasing steam pressure from 50% of normal operating pressure to the maximum steam pressure;
- Step 6 – Use JEDI software to determine the J-Integrals for the most onerous VCE direction.

The residual stress analyses used a mixed hardening material model, which was mapped from the uncracked model. The mixed hardening model combined the effects of isotropic and kinematic hardening. The isotropic hardening component expands the yield surface, whilst the kinematic hardening component shifts the yield surface according to the orientation of the loading. Therefore, the kinematic hardening makes the yield stress directional.

6.4.2. Analysis Approach for the Evaluation of J-Integrals

From the results of the residual stress comparison (discussed in Section 7), the following approach was used to evaluate the J-Integrals for the elastic-plastic cracked body analyses:

- Step 1 – Apply 100% normal operating system loads + full external pressure load (3.9 MPa, including crack face pressure) + 50% normal operating pressure (prevents any overclosure of the crack due to system loading), crack closed;
- Step 2 – As step 1 but with the crack open;
- Step 3 – Evaluate the J-Integral for pressures between 50% normal operating pressure and the maximum steam pressure.

Sensitivity analyses were performed with non-linear geometry (NLGEOM) set to 'off' and 'on'.

7. Results and Discussion

This section presents the results and discussion for the FE analysis of the manufacturing processes, in-service damage accumulations and critical defect sizes. Where available, test data have been compared to the results to assess the validity of the simulation.

7.1. Cold Forming

The following observations were made with respect to the geometric details and predicted equivalent plastic strains after cold forming:

- Figure 10 compares the predicted cross-section within the bent portion of the 1.5" pipe with that observed from a cut-up ex-service component. Equivalent plastic strains throughout the 1.5" pipe are also shown. The region of highest plastic strain at the intrados has a magnitude greater than 40% thus indicating extensive plasticity and material hardening;

- Equivalent plastic strains throughout the swaged 2" pipe are presented in Figure 11. They are shown to peak at regions either side of the two crotches. Due to the extent by which the swaged 2" pipe is deformed, extremely high plastic strains were observed with magnitudes greater than 70%. Similarly to the 1.5" pipe this indicates extensive plasticity and material hardening;
- The swaged 2" pipe wall thicknesses were predicted to be 4.96mm at the 0° crotch and 5.22mm at the flank positions. These compare well with measured values of 4.90mm and 5.36mm respectively thus giving confidence in the manufacturing simulation;
- The 1.5" pipe wall thicknesses were predicted to be 3.70mm at the 0° crotch and 4.12mm at the flank positions. These compare well with measured values of 3.79mm and 4.28mm respectively again giving confidence in the manufacturing simulation;
- The 1.5" pipe ovality was predicted to be 8.6%. This compares well with measured ovalities of up to 10%.

In summary, the fabrication models produced a good representation of the deformation of the components when compared to measurements made on real components.

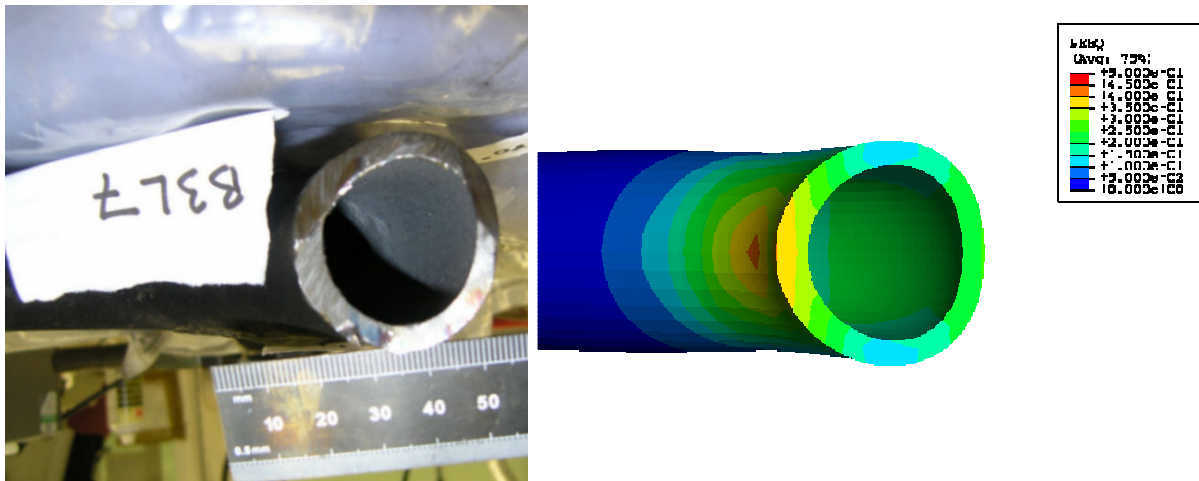


Fig. 10. Bent 1.5" Pipe Cross-Section Comparison (180°)

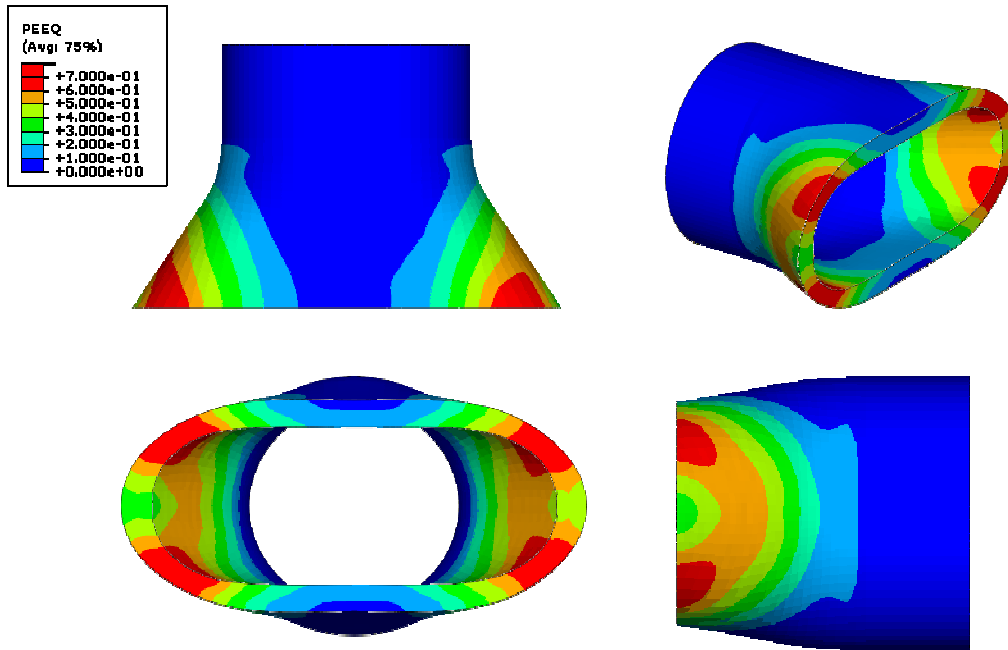


Fig. 11. Swaged 2" Pipe Equivalent Plastic Strains indicating regions of material hardening

7.2. Welding Analysis

Figure 12 highlights regions where significant plastic strain has accumulated and therefore regions where the material may have hardened. The figure indicates regions that are extensive in nature and suggest that the yield stress may vary significantly as a result of the cold forming process. It should be noted that variations in yield stress and presence of residuals stresses can influence the accumulation of creep and fatigue damage when in service..

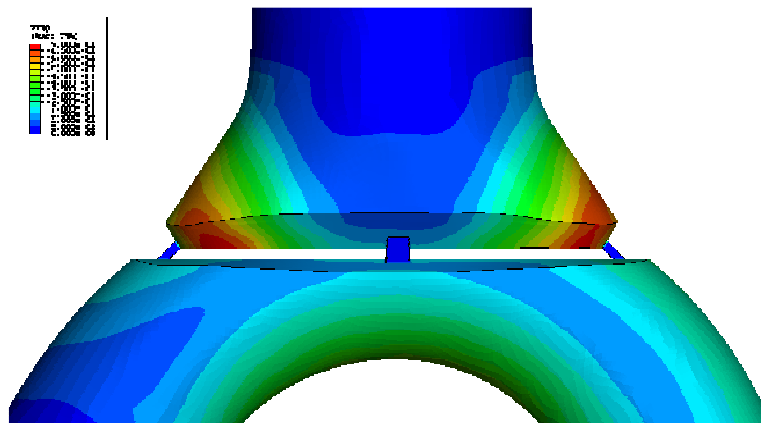


Fig. 12. Welding Model – Initial Plastic Strains Due to Cold Forming and Machining Operations

After simulation of the welding process predicted fusion boundaries for pass 1 and pass 2 were generated as shown in Figures 13 and 14 respectively. A blind comparison of the fusion boundaries with macrographs is shown in Figure 15. The purpose of the comparison was to provide confidence that the simulated welding process was representative of actual fusion boundaries measurements.

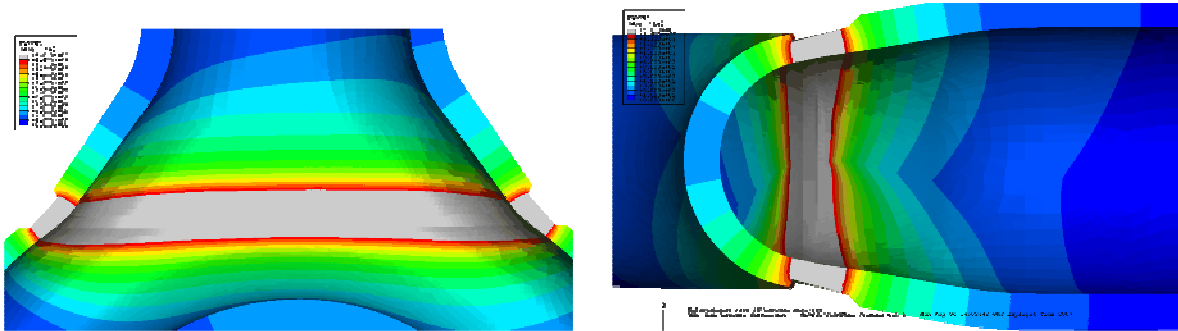


Fig. 13. Pass 1 Weld Fusion Boundaries Showing Extent of Melted Region

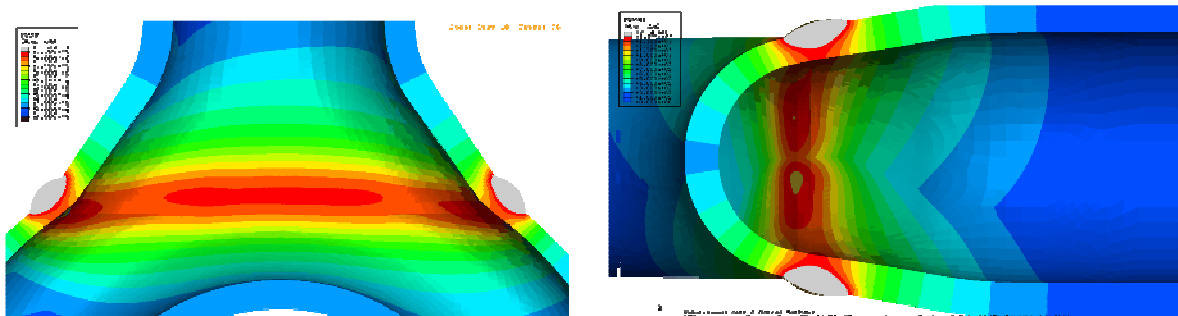


Fig. 14. Pass 2 Weld Fusion Boundaries Showing Extent of Melted Region

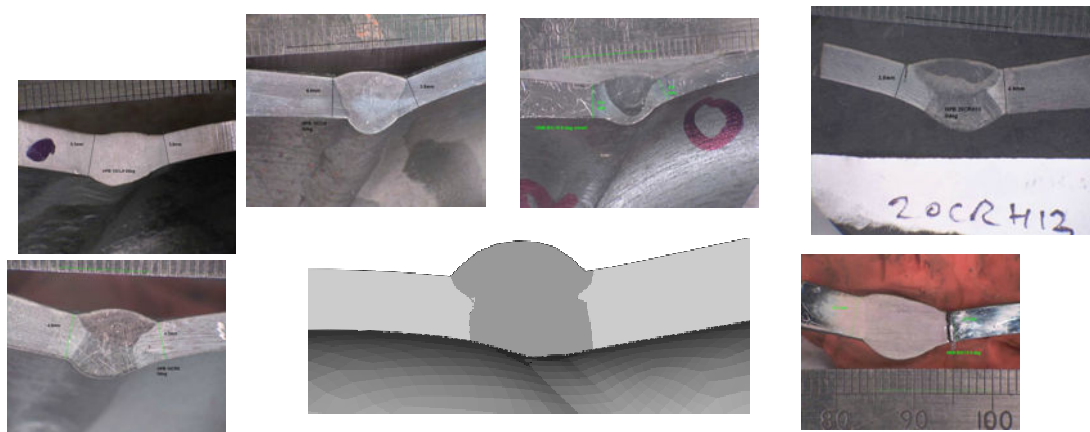


Fig. 15. Blind comparison of Macrographs and Total Fusion Boundary at the 0° crotch

High tensile transverse (150 to 250 MPa) and longitudinal (~450 MPa) residual stresses were predicted around the weld capping pass as shown in Figure 16 and Figure 17 respectively. These residual stresses are predicted to be present after welding but before PWHT. These locations are therefore a potential concern at the PWHT stage of manufacture since relaxation of these stresses results in the accumulation of creep damage which the component will contain before entering service.

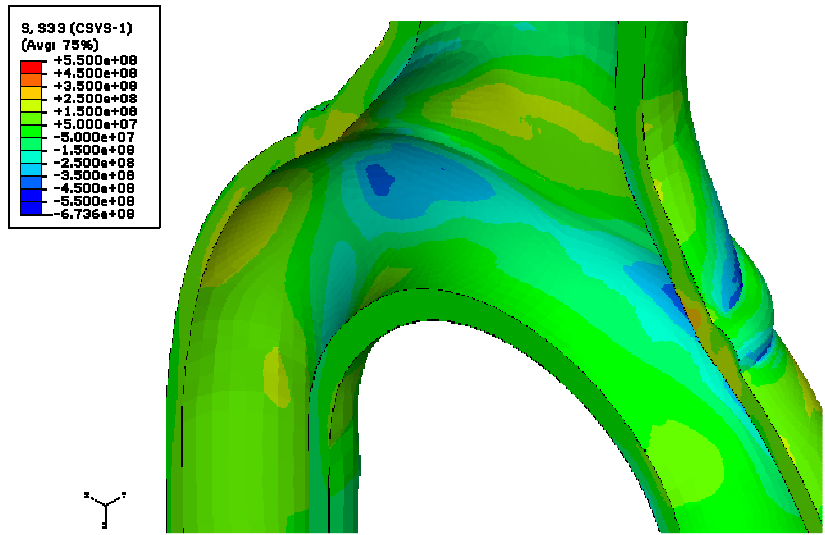


Fig. 16. Welding Global S33 Stresses ('Weld Transverse')

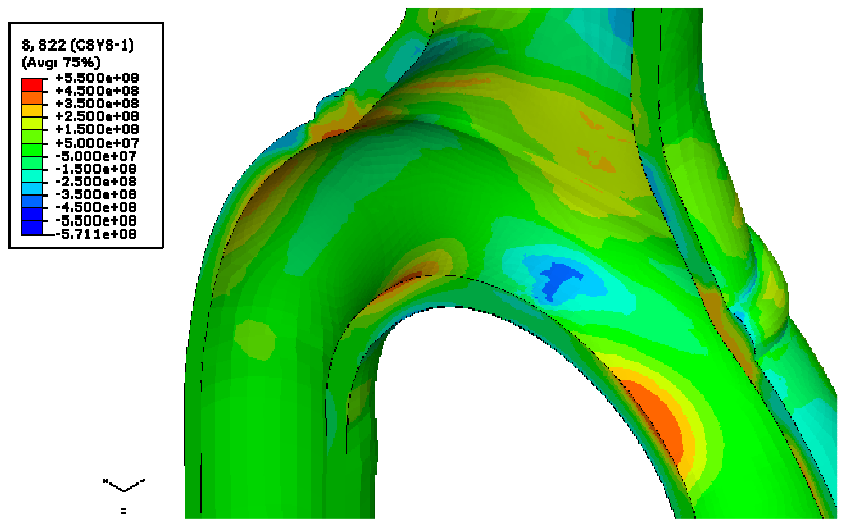


Fig. 17. Welding Hoop Stresses ('Weld Longitudinal')

As a result of the melting and re-solidification of weld and parent material around the weld excavation some of the earlier equivalent plastic strains (see Figure 12) were annealed, particularly within the fusion

boundary of the capping pass as shown in Figure 18. Equivalent plastic strains of up to 20% were observed underneath the capping pass due to welding.

The purpose of the residual stress simulation was to predict the magnitude of residual stress, material state and levels of plasticity within the component prior to PWHT.

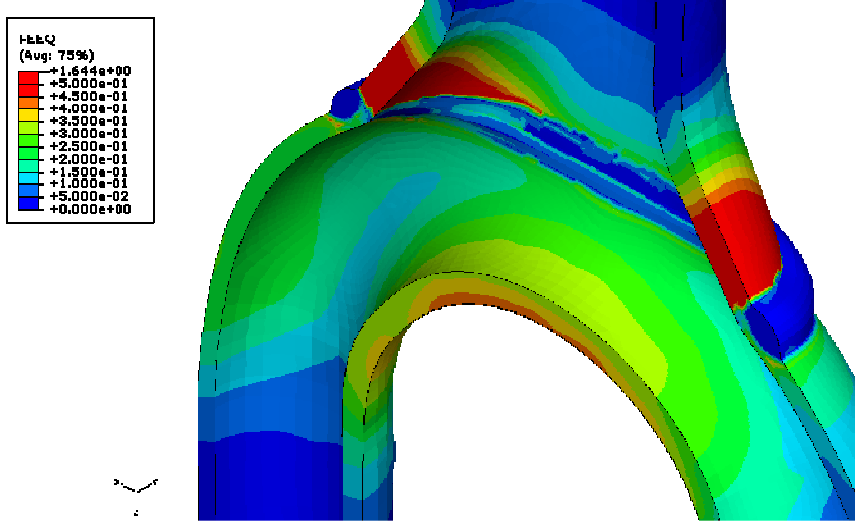


Fig. 18. Welding Equivalent Plastic Strains

7.3. PWHT

Figure 19 presents a banded contour plot of creep damage accumulated during PWHT. Mid-wall damage is shown in both the upper and lower HAZ of the two crotch positions, with a maximum magnitude of approximately 0.20.

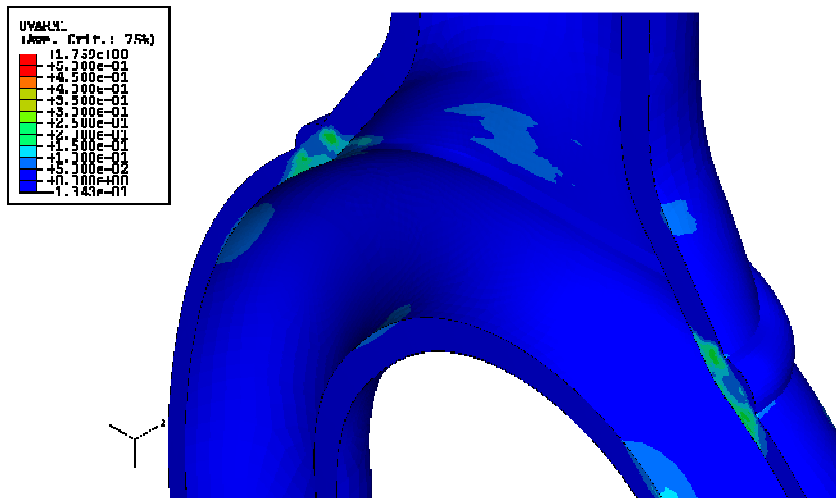


Fig. 19. Accumulated PWHT Creep Damage

The welding residual stresses were predicted to significantly decrease as a result of the PWHT. For all stress components the residual stresses were significantly reduced; the final von Mises stresses being typically less than 20 MPa and not exceeding 40 MPa.

The purpose of the PWHT simulation was to predict the stress, material and damage states within the component at start of life, for a subsequent structural integrity assessment of the component by consideration of it's through life creep-fatigue damage accumulation.

7.4. Creep-Fatigue Damage Analysis

Most of the in-service damage accumulation was predicted to occur at the flanks, with a large region of damage observed at the upper HAZ on both sides. This was mostly driven by the pressure loading. Figure 20 presents a quilt contour plot of creep-fatigue damage fraction accumulated during service. After 30 years (385 service cycles), peak damage was predicted at the flank upper HAZ on the outside surface, with a magnitude of 0.35.

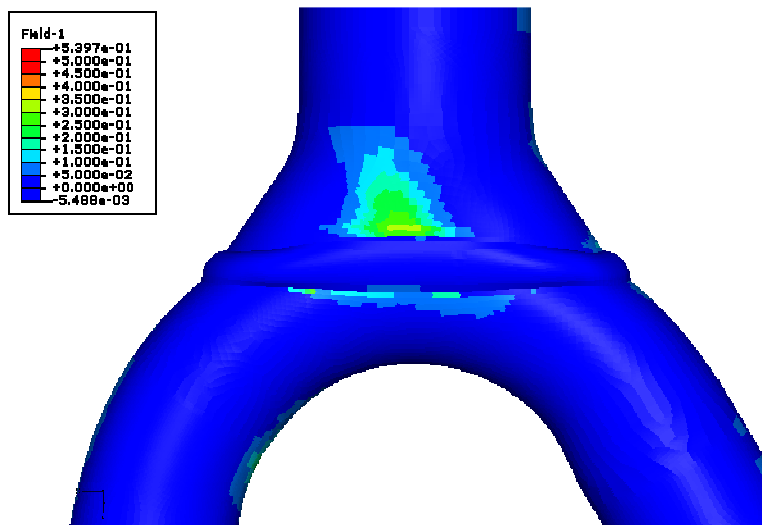


Fig. 20. Accumulated In-Service Creep-Fatigue Damage

Figure 21 shows the time history of creep-fatigue damage accumulation over the first 55 service cycles at the flank. The creep damage per cycle diminishes over time, but does not reach a steady state, suggesting that the flank remains in primary creep for at least 55 service cycles. The fatigue damage per cycle is negligible at the flank due to a low strain range throughout each cycle.

Crack initiation by creep-fatigue was not predicted to occur by modelling service cycles to 30 years.

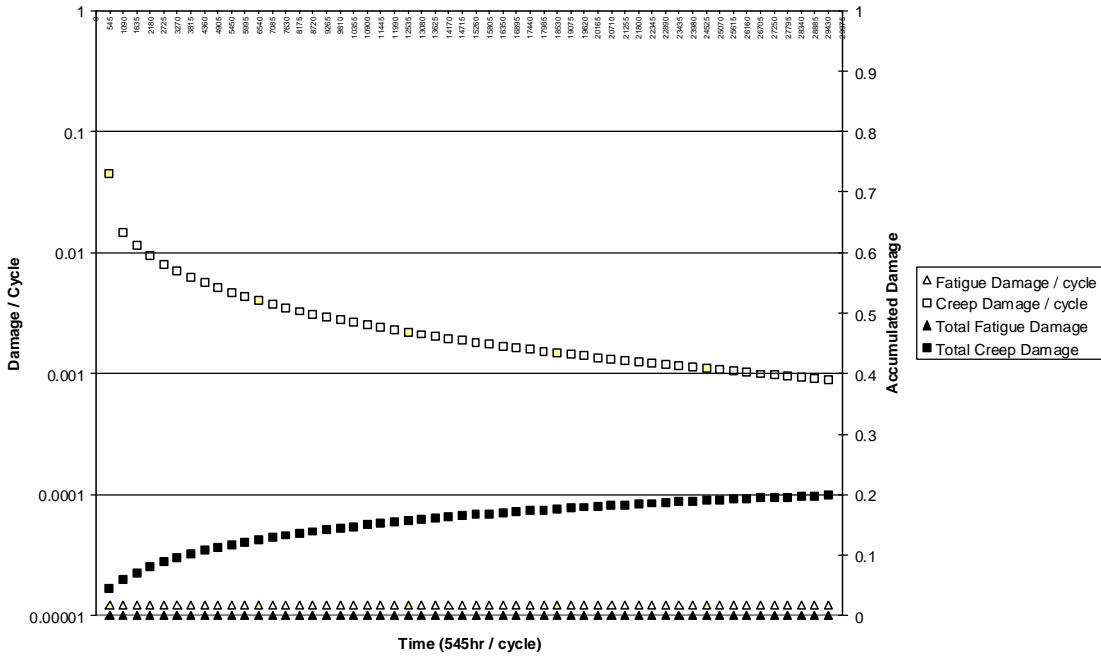


Fig. 21. Accumulation of In-Service Creep-Fatigue Damage at the Flank (First 55 Cycles)

7.5. Effect of Residual Stresses and Hardening on the J-Integral Evaluation

At the flank location, the plasticity under cyclic loading extended from the outer surface to approximately mid thickness (Figure 22). This reflected the extent of the hardening incurred during manufacture and to obtain a steady cyclic stress state. Only the shallowest crack size evaluated (1.5 mm deep) was subjected to any hardening at the crack tip (due to prior loading), where the tensile yield stress normal to the crack tip is increased by less than 1 MPa.

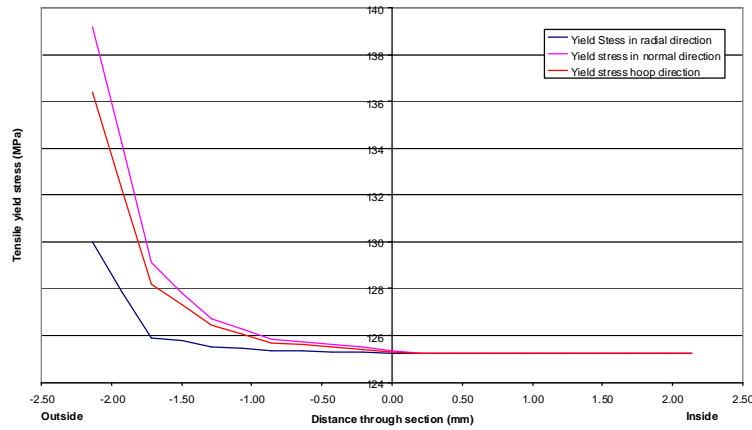


Fig. 22. Effect of cyclic hardening at the flank location

The J-Integrals for analyses with and without residual stress, evaluated using JEDI, are shown in Figure 23. The mode 1 residual stresses were compressive on the outer surface and as a consequence, the residual stresses slightly reduce the energy release rate. The effect of the residual stress was most significant at lower pressures, though it does persist at higher pressures. The highest J-Integrals were obtained by assuming there were no residual stresses and using the Abaqus results.

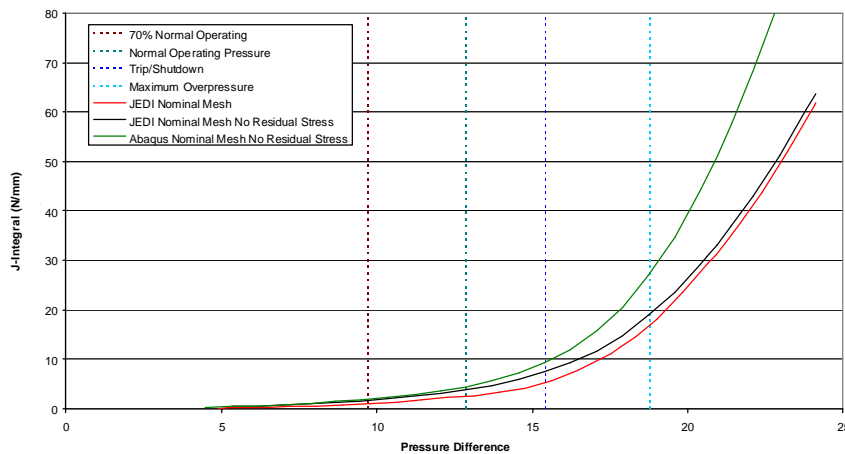


Fig. 23. Effect of residual stresses on the J-Integral evaluation at the flank, 2.3 mm deep crack

The residual stresses do not have a significant effect on the J-Integrals. Therefore, it was considered appropriate to evaluate the J-Integrals directly from Abaqus, without mapping across the residual stress state.

7.6. J-Integral Evaluation and Determination of the Critical Defect Size

The critical crack size was determined directly from the elastic-plastic J-Integral results. The system loads and external gas pressure were fixed whilst the steam pressure was ramped up to the maximum fault pressure. The variation of J with steam pressure was determined and then compared against the initiation fracture toughness to determine the critical pressure for each of the modelled defect sizes. The results for each discrete crack size were interpolated to obtain the critical crack size for a given steam pressure. In this case, the limiting lower bound initiation toughness at 550°C is 77 N/mm (Reference 6).

For each of the five crack sizes modelled, the most onerous VCE direction was direction 3. This represents an angle of 20° upward from the crack face (Figure 9) and was not considered to be sufficiently far from the parallel position to require changing the orientation of the crack plane.

J-Integrals were calculated for a number of element rings (contours) increasing in size from the crack tip. Path independence of the J-Integral evaluation was demonstrated by showing that convergence was obtained with increasing contours. Figure 24 shows that convergence was reasonable and that the highest J-Integrals occurred towards the deepest part of the crack. Note that Figure 24 uses results based upon a steam pressure of 28 MPa, which was higher than the maximum fault pressure of 24.1 MPa considered in the remainder of this paper.

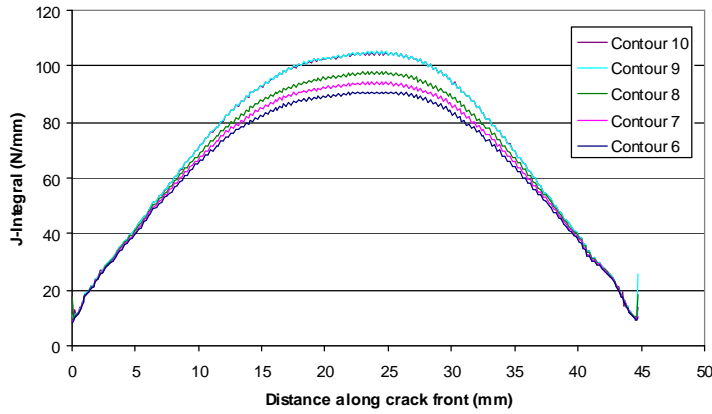


Fig. 24. Variation of J along a 2.3mm deep flank crack front for a pressure of 28 MPa

Figure 25 shows the variation of J-Integral with the pressure differential for each of the five crack depths considered. The critical defect sizes were calculated by comparing the elastic-plastic J-Integral results with the lower bound initiation toughness at the operating pressures being considered. For example, for the maximum steam pressure of 24.1 MPa, a crack depth of 3.1 mm can be tolerated by the component given an initiation toughness of 77 N/mm (Figure 25).

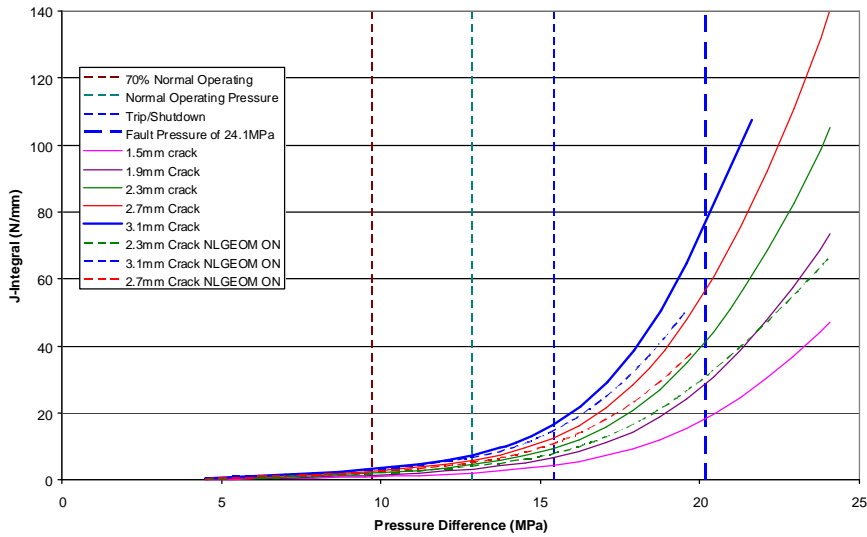


Fig. 25. Elastic-plastic J-Integrals at the flank location

The majority of analyses were carried out without non-linear geometry. Lower J values were calculated where non-linear geometry was used (Figure 25). However at high loads, the contour convergence of non-linear geometry was poor and hence the results were less reliable. In addition, the status of J evaluated

using non-linear geometry was unclear with respect to its application for performing fracture assessments. Therefore, the results calculated using linear geometry were considered to be the most appropriate.

8. Conclusions

A comprehensive assessment of the structural integrity of a pipework joint has been assessed in this paper. It describes a simulation of the manufacture, through-life operation and limiting defect size assessment. A range of factors have been considered to investigate their influence on the integrity of the joint in-service to support accurate predictions of service life. This work differs from typical structural integrity assessments in that advanced modeling techniques have been used through-out the assessment process.

The main conclusions that were made for this study are summarised below:

- FE modeling of cold forming and welding operations for a pipework joint were undertaken which were able to successfully represent the fabrication process as demonstrated by comparisons with test data;
- Significant residual stresses were predicted following an assessment of the cold forming and welding process;
- PWHT significantly reduced the residual stresses to less than 40 MPa. The relaxation of residual stresses resulting in the accumulation of creep damage of ~ 0.25 in the mid-wall at the crotch lower and upper HAZ;
- In-service damage accumulation occurred at the flanks, with a large region of damage observed at the upper HAZ on both sides. This was mostly influenced by the pressure loading;
- The accumulation of fatigue damage was insignificant in comparison to the accumulation of creep damage;
- The maximum creep-fatigue damage after 30 years of simulated operation (385 cycles) was predicted to be approximately 0.35 at the flank upper HAZ;
- Crack initiation by creep-fatigue was not therefore predicted to occur by simulating service cycles to 30 years;
- Residual stresses were shown not to have a significant influence on the critical defect size within the pipework joint;
- The variation in J with increasing steam/gas pressure differential pressure was reported. By comparing these curves with the initiation J, a critical pressure can be determined for each crack size. Hence, the critical defect size for known operational pressure differentials can be calculated by interpolation between these curves.

The outcome of this work greatly enhanced our knowledge of the behaviour of the pipework joint and the factors that influence its in-service integrity.

Acknowledgements

The work was funded by EDF Energy Nuclear Generation Ltd. and this paper is published with its permission.

References

- [1] An Assessment Procedure for the High Temperature Response of Structures, British Energy Generation Ltd., R5 Issue 3, June 2003.
- [2] Abaqus User's Manual, SIMULIA, Inc., Version 6.7, 2007

- [3] N A Leggatt, Finite Element Weld Simulation Of The TRAINSS Repair Weld, Frazer-Nash Consultancy Report FNC 31892/005/31562R, Issue 1, September 2006.
- [4] P J Bouchard, 1998, VORSAC WP 2 Task 2.2.1: Material Properties for AISI Type 316 Stainless Steels and Type 316L Weld Metal, Nuclear Electric Report EPD/GEN/REP/0240/97, VORSAC(98)D004.
- [5] M C Smith, Hartlepool and Heysham 1 power stations: Development of mixed isotropic-kinematic material hardening models for finite element simulation of austenitic steel welds, British Energy Report E/REP/BDBB/0092/AGR/06, Revision 000, 2006.
- [6] AGR Materials Data Handbook R66, British Energy Generation Ltd, Rev. 007, December 2008.
- [7] R J Dennis, Development of Generalised three-dimensional Creep ABAQUS Subroutines for Temperature Dependent Ductility, Frazer-Nash Report 5603-3/2968RB, Issue 1, September 2003.
- [8] J O'Neill, Residual Stress and Creep Damage Simulations of Repairs in 19mm and 35mm (AISI 316H) Boiler Spine Welds, Frazer-Nash Report FNC 5603/30288R, Issue 1, June 2003.
- [9] Gieck, Engineering Formulas, Eighth Edition, McGraw Hill, Table Z7.
- [10] A Kwong and N A Leggatt, FEAT Weld Heat Source Modelling Tools: A General Overview, Frazer-Nash Consultancy Report FNC 5603/12/3374RB, Issue 1 (2004).
- [11] FEAT Weld-Modelling Tool (WMT) User Guide, FEATPLUS Limited, Version 1.0.8, FP/CR/0019/06 Issue 1, March 2006.
- [12] E G Sinclair, Re-evaluation of System Loading on Secondary Superheater Bifurcation and Tailpipe to Pintle Welds at Full Power Operating Conditions, EASL Report BE-TSA/1125/07, Issue 1, December 2007.